Characterization of NRC Convair-580 hot-wire probes performance using NRC AIWT

Fleury, Liam; Bliankinshtein, Natalia; Nichman, Leonid; Bala, Kenny; Wolde, Mengistu

Laboratory Technical Report (National Research Council of Canada. Flight Research Laboratory); no. LTR-FRL-2021-0132, 2023-01-18

NRC·CNRC

Flight Research – Aerospace Research

Characterization of NRC Convair-580 hot-wire probes performance using NRC AIWT

LTR-FRL-2021-0132

18 January 2023

Author/Auteur: **Liam Fleury – NRC, Natalia Bliankinshtein – NRC, Leonid Nichman – NRC, Kenny Bala – NRC, Mengistu Wolde – NRC**

National Research Council Canada | Conseil national de recherches Canada

Canada

FLIGHT RESEARCH LABORATORY

Characterization of NRC Convair-580 hot-wire probes performance using NRC AIWT

Report No.: LTR-FRL-2021-0132

Date: 18 January 2023

Authors/Auteurs: Liam Fleury – NRC, Natalia Bliankinshtein – NRC, Leonid Nichman – NRC, Kenny Bala – NRC, Mengistu Wolde – NRC

Classification :	Unclassified	**Distribution :**	Limited
For:			
Reference:			
Submitted by:	Natalia Bliankinshtein		
Approved by:	Kirk Shaw, **Director**		

Pages : 45	**Copy No : 1**
Fig. : 17	**Diagrams : 0**

Abstract

This laboratory technical report presents the results of bulk cloud water content measurements taken with the Ice Crystal Detector and Nevzorov probes at the Altitude Icing Wind Tunnel of NRC.

The Nevzorov and Ice Crystal Detector are aircraft-mounted hot-wire probes designed to find the bulk water content of clouds and are being used as the NRC Convair 580 aircraft core sensors. These two probes were tested in the NRC Altitude Icing Wind Tunnel facility in late 2020 and early 2021 in order to characterize their responsiveness to liquid water in a controlled environment. The probes were tested at a variety of liquid water content set points, particle median volume diameter, true air speed, pressure, and temperature. Measurements of the liquid water content and total water content were made in a setting of pure liquid conditions, and the probes measurements were compared to wind tunnel nominal values. The calculation of dry power loss for the Ice Crystal Detector was improved using a modified fit in the clear air. Icing was observed on both Nevzorov reference wires, creating a false signal and unreliable data, leading to the conclusion that the dry power loss should be calculated using the ambient parameters similar to how it is done for the Ice Crystal Detector.

Table of Content

List of figures 7
List of Tables 7
List of Acronyms 7
1. Introduction 8
2. Experimental Setup 10
2.1 AIWT Facility Description 10
2.2 AIWT Icing Spray System 11
2.3 Installation of Hot-Wire Probes 12
3. Data Processing and Analysis Methodology 12
3.1 ICD Data Processing 12
3.1.1 Retrieval of WC from the Raw Signal 12
3.1.2 Dry Term Improvement 13
3.2 Nevzorov Data Processing 14
3.2.1 Retrieval of WC from the Raw Signal 14
3.2.2 Dry Term Improvement 16
3.3 Analysis of Sensor Responsiveness in Wind Tunnel 18
4. Results and Discussion 20
4.1 Sensor Responsiveness in LWC Sweeps 20
4.2 Sensor Responsiveness in MVD Sweeps 24
4.2 Effect of Icing on Nevzorov Probe 29
4.3 Cloud Masking Unreliability in Nevzorov Calculations 33
4.4 Error Analysis 34
5. Conclusions 36
Acknowledgments 37
Appendix A 38
Appendix B 39
Appendix C 40
Appendix D 41
References 44

List of figures

Figure 1. Schematic of the NRC's AIWT facility (Courtesy AIWT). 11
Figure 2. MVD 10 µm, TAS 90 m/s LWC Sweep. 20
Figure 3. MVD 20 µm, TAS 80 m/s LWC Sweep 21
Figure 4. MVD 20 µm, TAS 80 m/s, Pressure 70 kPa LWC Sweep 21
Figure 5. MVD 100 µm, TAS 80 m/s LWC Sweep. 22
Figure 6. MVD 250 µm, TAS 80 m/s LWC Sweep. 23
Figure 7. LWC 0.2 g m^{-3}, TAS 100 m/s MVD Sweep. 24
Figure 8. LWC 0.2 g m^{-3}, TAS 90 m/s MVD Sweep 25
Figure 9. LWC 0.5 g m^{-3}, TAS 80 m/s MVD Sweep 25
Figure 10. LWC 0.5 g m^{-3}, TAS 90 m/s MVD Sweep. 27
Figure 11. LWC 0.7 g m^{-3}, TAS 90 m/s MVD Sweep. 27
Figure 12. LWC 1.5 g m^{-3}, TAS 90 m/s MVD Sweep. 28
Figure 13. Ice contact with Nevzorov reference wire. 30
Figure 14. Power loss due to icing on Nevzorov LWC reference wire. 31
Figure 15. Signal due to icing on Nevzorov TWC reference wire. 32
Figure 16. a and b. Ice falling off Nevzorov leading to anticorrelation of false signals on LWC and TWC reference wires. 32
Figure 17. Anticorrelation of false signals on LWC and TWC reference wires. 33

List of Tables

Table 1. Coefficients found for 4 wires of Nevzorov using Eq. 11. 16
Table 2. MVD and LWC sweeps information. 19
Table 3. Uncertainty due to dry air power loss. 35

List of Acronyms

AIWT Altitude Icing Wind Tunnel

AL Aerodynamics laboratory

APDC Aeronautical Product Development and Certification

DAS Data Acquisition System

FAA Federal Aviation Administration

FRL Flight Research Laboratory
GLAZEICE Ground Level and Airborne sub-Zero Experimentation for In-cloud Characterization Effectiveness
ICD Ice Crystal Detector
IWC Ice Water Content
LWC Liquid Water Content
MSE Mean Squared Error
MVD Median Volume Diameter
PSD Particle Size Distribution
SAT Static Air Temperature
SEA Science Engineering Associates Inc
SP Static Pressure
TAS True Airspeed
TAT Total Air Temperature
TWC Total Water Content
WC Water Content

1. Introduction

Hot-wire probes are a class of widely used instruments for measuring cloud water content (WC). Unlike other types of airborne probes capable of measuring WC, such as imaging or scattering probes that infer WC from particle-by-particle measurements, constant-temperature hot-wire probes can measure the WC directly from the power dissipated by melting and evaporation of hydrometeors. Hot-wire probes facilitate real-time monitoring of WC information in flight, while other types of probes usually require post-processing and significant data scrutiny before these parameters can be confidently calculated.

Two hot-wire probes, the Ice Crystal Detector (ICD) and Nevzorov, are extensively used for atmospheric research flight campaigns onboard the NRC Convair-580 aircraft. The total and liquid water contents (TWC and LWC) measured by them, also known as the bulk properties, are one of the core microphysics parameters collected in research flights and therefore need to be accurately measured.

The Nevzorov probe (Korolev et al 2013) is a commonly used hot-wire probes that is designed for aircraft measurements of the ice water content (IWC) and LWC of clouds. The probe has two heated collector elements sensitive, respectively, to liquid hydrometeors and all hydrometeors, thus enabling phase separation and identification of liquid, mixed-phase and glaciated clouds. A distinguishing feature of the Nevzorov probe is two reference wires, which are similar in geometry to the collector wires, but shielded from the airflow so their power loss provides a “dry term” (i.e. all cooling influences except the interception and evaporation of hydrometeors). Therefore, in theory, Nevzorov probe can serve as a stand-alone probe, not requiring other data such as ambient temperature, pressure and true airspeed. In practice, the reference wires have been shown to be unreliable, as further explained in Section 4 of this report.
The ICD probe by Science Engineering Associates (SEA, Lilie et al., 2016) applies the same principles as the Nevzorov probe but has a different collector element shape and no reference wires. The ICD TWC and LWC sensors have similar cylindrical shapes, with one of them being convex to deflect ice particles and the other concave to capture all hydrometeors. The ICD requires the knowledge of ambient atmospheric parameters to estimate the ‘dry power’ term which needs to be subtracted from the total power dissipated on the collector wires.

In flight campaigns conducted in 2018-2019 (Bernstein et al., 2021; Nguyen et al., 2022), the NRC Convair-580 mission scientists noticed a range of potential issues with the probes performance, including electric noise of unknown origin, disagreement in WC measurements between the ICD and Nevzorov, and non-physical artifacts such as negative IWC (a result of TWC < LWC) in certain flight environments. This motivated the need for a detailed study of sensor performance in a controlled environment, such as can be created in a wind tunnel. The NRC Aerodynamic Laboratory (AL) Altitude Icing Wind Tunnel (AIWT) hosted the experiment and provided a flexible testing environment representative of realistic flight conditions thanks to a wide range of available speeds, temperatures, altitudes (pressures) and water spray parameters. These tests were performed from September 18th-September 21st 2020, December 3rd 2020 and February 10th 2021.

The goal of this document is to provide a quality assessment of the operation of bulk probes, which are currently used in airborne missions and to report measured quantities that may help in the characterization of AIWT performance. The report compares sensor responses in various conditions (different set-points of LWC, MVD, static pressure, static temperature, true air

speed), complemented with comparison between the two hot-wire sensors, and in relation to the nominal AIWT readings (derived from calibrations with rotating icing cylinder (Clark, 2021)).

2. Experimental Setup

2.1 AIWT Facility Description

A schematic of the NRC AIWT facility is depicted in Figure 1. It is a refrigerated closed-loop low-speed facility oriented in the vertical plane. Being refrigerated, this facility can be used any time of the year to conduct icing tests in accordance with the icing conditions of *Appendix* C to Part 25 of the #14 Code of Federal Regulations of the Federal Aviation Administration (FAA (2021)).

The standard test section in the AIWT is 0.57 m × 0.57 m × 1.83 m (width × height × length), and has controlled airspeeds from 5 to 100 m/s. An insert can reduce the test section width to 0.52 m and height to 0.33 m to achieve airspeeds up to ~180 m/s. The tunnel airspeed is calculated through the use of total temperature and total pressure sensors located upstream of the spray bars in the settling chamber, as well as a ring of static pressure ports located upstream of the AIWT test section.

The air temperature in the AIWT is controlled by varying the amount of the refrigerant passing through a heat exchanger located in the tunnel circuit; achievable static air temperatures (SAT) at a Mach number of 0.3 ranges from -40 ºC to +30 ºC. A vacuum pump can be used to evacuate air from the wind tunnel circuit, lowering the pressure and creating simulated flight altitudes up to 12,200 m (40,000 ft). More technical details and specifications of the NRC icing facility can be found in LTR-AL-2021-0018 (Clark, C., 2021).

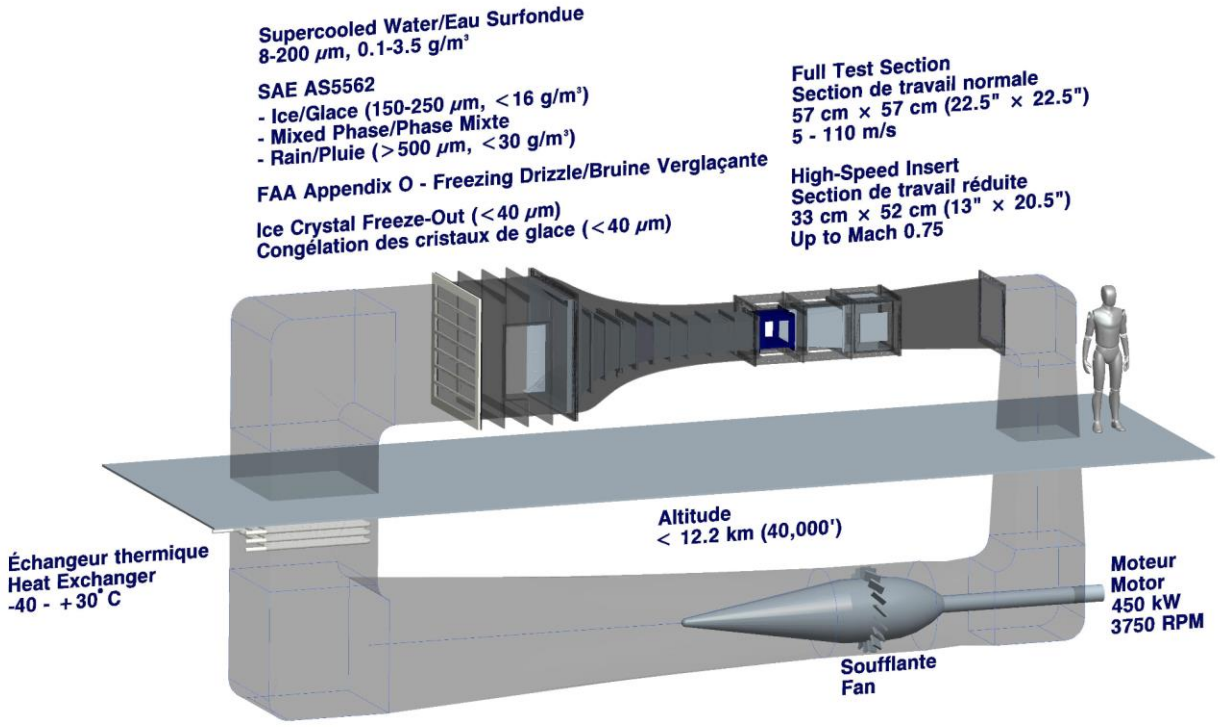

Figure 1. Schematic of the NRC's AIWT facility (Courtesy AIWT).

2.2 AIWT Icing Spray System

The icing spray system combines the outputs from air-supply and water-supply sub-systems through the use of individual air lines to each spray bar and individual water lines to each spray nozzle. The spray nozzles are mounted on the icing spray bars, which are located in the tunnel's settling chamber, downstream of the flow straightening honeycombs and turbulence reducing screens. There are six horizontal spray bars spaced evenly over the settling chamber height. The spray system is monitored and controlled by the wind tunnel control system.

A still provides distilled water to a heated water reservoir. This water is then pumped to a spray bar header using a variable-frequency motor drive to maintain constant water pressure. The water supply line for each spray bar includes a flow controller to permit equalizing of the water flow for all of the spray bars. The total water flow to the spray bar system is monitored using a Coriolis mass flow meter. A computer-controlled air-pressure regulator controls the air pressure to the spray bar air header. Both the total water flow and the total air flow through the systems are monitored using Coriolis mass flow meters.

2.3 Installation of Hot-Wire Probes

Each probe was tested in the AIWT individually in order to mount each probe on the centerline of the test section and avoid blockage interference effects. The icing cloud distribution in the AIWT is provided in Appendix A. The sensors tested were the SEA ICD, serial number 4005, and a standard 8mm cone Nevzorov, serial number 300.

Two data acquisition systems (DAS) were used, AL's AIWT DAS recorded direct measurements and calculated parameters of the facility, such as MVD, LWC, SAT, etc., while FRL's M300 DAS (Rigol 2015) was used to acquire and record hot-wire probe data, and a few data parameters transmitted over the network from the AIWT DAS (SAT, TAS and pressure). A schematic of the data acquisition system is provided in Appendix B.

3. Data Processing and Analysis Methodology

3.1 ICD Data Processing

3.1.1 Retrieval of WC from the Raw Signal

The data processing for this experiment was done in Matlab R2021b. The raw data was processed by first calculating the power loss of each sensor given as:

$$P = IV \tag{1}$$

Where *P* is the power loss, *I* is the sensor current and *V* is the sensor voltage. A power correction is then applied to adjust for the resistance of the fixture (SEA, 2016). The corrected power is:

$$P_{corrected} = \frac{P_{total}\left(R_{total} - R_{fixture}\right)}{R_{total}} \tag{2}$$

Where R_{total} and $R_{fixture}$ are the total and fixture resistances, respectively. The new, corrected power is the total power loss of the sensor, given in terms of the wet and dry power as:

$$P_{corrected} = P_{dry} + P_{wet} \tag{3}$$

In order to isolate the wet power, which is the power loss due to water presence, a dry power term is required that represents the amount of power the sensor will lose in dry air. This dry power term is based on the ambient conditions and methods to calculate it are discussed in section 3.1.2. This dry power is then subtracted from the total power in order to determine the wet power. From this wet power, the water content is given as (SEA 2016):

$$LWC = \frac{P_{wet} \cdot 2.389 \times 10^5}{[L_{evap} + (T_{evap} - T_{ambient})] \cdot TAS \cdot A_{sense}} \quad (4)$$

where P_{wet} is power in watts, L_{evap} is the latent heat of evaporation of water, given in $\frac{cal}{g}$, T_{evap} is the temperature when water evaporates at a given pressure, and A_{sense} is the sensor area in mm^2. The sensor area, obtained in the most recent calibration in January 2021, is 24.21 mm^2 for the STWC (concave) sensor and 23.955 mm^2 for the S083 (convex) sensor. Since the wind tunnel data is made up of entirely liquid water, no further processing is required to separate the liquid water content from the ice water content.

3.1.2 Dry Term Improvement

One goal of this analysis is to improve the dry air term. To do this, the points without any water in the flow were isolated based on the AIWT DAS LWC output. These points were reviewed manually to remove any points with undesired conditions or behaviour (e.g., wind tunnel turned off to adjust instruments, transient effects were present, etc.).

Once the data was refined, a few different approaches of data selection were used. The first approach was to take every point in the dataset and weigh it equally, then fit a curve to the data. Using this strategy, fits were found for the LWC and TWC with an R^2 of 0.9268 and 0.9392, respectively. While most of the data were taken in similar conditions, with infrequent variations in pressure and TAS, and the fitted curve was found to be very effective in the most common conditions, in less tested conditions the fitted curve didn't represent the data well. . The second strategy that was tried was to use a 30 minute dedicated dry run where the pressure and temperature were controlled. The fit was not improved using this strategy, as the pressure and temperature were varied simultaneously there was not enough data for the fit to represent the whole data set. It was found that the most effective strategy was to assign every point a weight, where the aforementioned 30 minute period was weighed twice as much as other points. This led to a fit being found with an R^2 of 0.9282 for the LWC sensor and 0.9417 for the TWC sensor, a small improvement over the standard weighing strategy.

The other issue with the dry term fit was the form of the fit. The formula given by the user manual (SEA 2016) is:

$$P_{dry} = a \cdot (T_{sense} - T_{ambient}) \cdot (P_{ambient} \cdot TAS)^b \quad (5)$$

The fit from this formula was unsatisfactory with the manufacturer-recommended initial coefficients, and so in order to improve this an offset term was added and the formula became:

$$P_{dry} = a \cdot (T_{sense} - T_{ambient}) \cdot (P_{ambient} \cdot TAS)^b + c \quad (6)$$

This was better with the initial coefficients used, giving an R^2 of 0.9252 for the LWC sensor and 0.8726 for the TWC sensor, but rather than a constant offset, a more theory-driven modification was desired. A modification using Reynold's numbers and Nusselt's numbers was made (King, 1978; McFarquhar et al., 2017) and the final formula used is:

$$P_{dry} = a(T_{sense} - T_{ambient}) \cdot (\frac{P_{ambient} \cdot TAS}{T_{film} + 273.15})^b \quad (7)$$

Where T_{film} is the average of the sensor and ambient temperature.

This formula was used for a curve fit with R^2 of 0.9282 for the LWC sensor and 0.9417 for the TWC, which is an improvement over the other two strategies. This formula was used to process the data presented in section 4. The final values for the coefficients were determined to be a = 0.005155, b = 0.33 for the LWC sensor and a = 0.005742, b = 0.3249 for the TWC sensor.

3.2 Nevzorov Data Processing

3.2.1 Retrieval of WC from the Raw Signal

Unlike the ICD, the Nevzorov probe has two reference wires, one associated with each of the LWC and TWC sensors. Although the dry term can be calculated from the ambient parameters, much like it is for the ICD, making use of the reference wires, the dry term for the Nevzorov probe is calculated as:

$$P_{dry} = K \cdot P_{reference} \quad (8)$$

Where $P_{reference}$ is the power loss in the reference wire, and K is a proportionality factor given as the ratio between the reference wire power loss and sensor wire power loss in dry air. There are two ways to calculate this ratio in clouds. The first is by interpolating the data from the pre-

test point and post-test point clear-air points. This strategy uses the most recent known value of K before the sensor enters the cloud, or in the case of the wind tunnel before the water spray is turned on. This strategy is the primary strategy used to determine *K* but it is unreliable in longer clouds, or when the altitude is changing within a cloud (Abel et al., 2014). Since *K* is dependent on the conditions of the environment, any change to the environment introduces an offset bias.

Once the dry term is calculated and subtracted from the total power to find the wet power, the WC can be calculated. Since there is a known IWC of 0 g m^3 in the AIWT, this simplifies the calculation of the LWC. The LWC is then given as:

$$LWC = \frac{P_{wet}}{\epsilon \cdot TAS \cdot A_{sense} \cdot L_{evap}} \quad (9)$$

Where $\epsilon$is the efficiency of the sensor, which is dependent on the MVD, $A_{sense}$is the sensor area in cm^2, given as 0.324 cm^2 for the LWC sensor and 0.502$cm^2$for the TWC sensor. L_{evap} is the latent heat of evaporation for water (see Appendix C). This latent heat of evaporation is approximated as 2589 $\frac{J}{g}$. This approximation, recommended by the User Manual (SkyPhysTech Incorporated), imposes a 5% uncertainty on the calculated LWC from -40 ℃ to 20 ℃. The LWC was calculated for each sensor independently in order to compare the responsiveness of the two sensors.

One significant difference between the Nevzorov and ICD is the known low-collection efficiency of the Nevzorov. For small droplets (MVD < 20 μm) the TWC and LWC sensors both have a low collection efficiency. The first approximation for the collection efficiency is given as (Korolev et al., 1998):

$$\epsilon = \frac{{d^2}_{eff}}{{d^2}_{eff} + {d_0}^2} \quad (10)$$

Where d_{eff} is the effective diameter of the droplet, which is considered to be equivalent to the median volume diameter (Cober and Isaac, 2012) and d_0 is a constant coefficient, unique to each sensor. For the LWC sensor d_0 is 1.7 μm and for the TWC sensor d_0 is 7.5 μm (Korolev et al., 1998). This collection efficiency only applies at speeds on the order of 100 m/s. This is faster than the wind tunnel speeds, which are 80 m/s and 90 m/s in the sweeps. This formula appears to be the most recent estimation of LWC collection efficiency based on the sensor geometry, but there is an improved estimation of the TWC efficiency from the NASA LEWICE model (Strapp et

al. 2003). It appears that Eq.10 underestimates the collection efficiency by approximately 15% at 10 μm, but is fairly accurate at 20 μm. If the collection efficiency of the LWC sensor behaves similarly to that of the TWC, the difference in collection efficiency from 1 is likely negligible, as Eq. 10 suggests that the LWC efficiency should be 97 % at 10 μm and 99.3 % at 20 μm. So, while the efficiency for the TWC element is estimated to be 75 % at 10 μm and 87 % at 20 μm and therefore must be adjusted, the LWC-element results are not adjusted for efficiency.

While estimates of the sensor collection efficiencies for large particles exist in the literature, no correction for those was applied in this analysis for either of the probes. As the AIWT tests presume only liquid particle, ideally, TWC and LWC sensor readings should match. Any discrepancy between the readings from the two elements indicates a difference in their collection efficiencies.

3.2.2 Dry Term Improvement

As noted in the previous section, the dry air term for the Nevzorov probe is traditionally determined based on the ratio of the power loss between the collector and reference wires. This ratio, *K*, can be determined either by interpolation or a calculation based on atmospheric conditions. Similar to the dry power fit for ICD, it is possible to find the power dissipated on a reference wire (and on a collector wire in clear air, with appropriate a and b coefficients) using Eq. 11:

$$P_{dry} = a(T_{sense} - T_{ambient}) \cdot \left(\frac{P_{ambient} \cdot TAS}{T_{film}+273.15}\right)^{b} \quad (11)$$

A fit of this form was found successfully for all four wires, with the coefficients and R^2 values shown in table 1:

Table 1. Coefficients found for 4 wires of Nevzorov using Eq. 11.

Wire	a value	b value	R^2
LWC Sensor	0.006359	0.4635	0.9762
LWC Reference	0.00275	0.5152	0.9637
TWC Sensor	0.00998	0.2325	0.8981

TWC Reference	0.00105	0.7202	0.9809

Taking a ratio between fits of this form shows that the ratio between the sensors dry power loss can be represented as:

$$K = a\left(\frac{P_{ambient} \cdot TAS}{T_{film}+273.15}\right)^{b} \quad (12)$$

A fit of this form was successful for the TWC sensor (R^2 of 0.95) with the coefficients a_{TWC} = 9.833 and b_{TWC} = -0.4942 but unsuccessful for the LWC sensor (R^2 of 0.48) with the coefficients a_{LWC}= 2.291 and b_{LWC} = -0.04992

Another way to calculate K is described in Abel et al. (2014) as:

$$\Delta K = a_{IAS}\Delta\left(\frac{1}{V_{IAS}}\right) + a_P \Delta log_{10}(P) \quad (13)$$

In order to calculate K, as opposed to the change in K, the following formula was used:

$$K = K_0 + a_{IAS}\left(\frac{1}{V_{IAS}} - \frac{1}{V_0}\right) + a_P\left(log_{10}(P) - log_{10}(P_0)\right) \quad (14)$$

where K_0 is the median true value of K in the data set, V_0 is the indicated air speed when K = K_0 and P_0 is the pressure when $K = K_0$. The coefficients a_{IAS} and a_P given in Abel et al. (2014) are a_{IAS} = 30.0 and a_P = -0.29. Using these coefficients an R^2 of 0.85 was found for the TWC sensor, and an R^2 of 0.495 for the LWC sensor. This indicates that the fit is decent for the TWC sensor, but very poor for the LWC sensor. When calculating a_{IAS} and a_P automatically in the curve fit, the quality of fit for both of these sensors improved to an R^2 of 0.94 with coefficients for the TWC sensor and 0.52 for the LWC sensor.

The quality of the fit for K (LWC sensor) appears to be significantly worse than for the TWC sensor, but this is due to the fact that there is very small variation in the value of K_{LWC}. When using this K in conjunction with the reference wire power to predict the sensor power in dry air, an R^2 of 0.97 is found. Ice buildup was observed touching the LWC reference wire, leading to direct power loss (see Section 4.2). Therefore direct calculation is the preferred way of calculating the dry air power loss as given by:

$$P_{LWCdry} = 0.006359(T_{sense} - T_{ambient}) \cdot \left(\frac{P_{ambient} \cdot TAS}{T_{film}+273.15}\right)^{0.4635} \quad (15)$$

This equation is also recommended for use in flight data analysis, where the LWC reference wire is similarly subject to icing in flight conditions.

Although it is less frequent, the TWC reference wire is also vulnerable to icing in certain conditions. This is discussed in-depth in section 4.2, and the preferred way of calculating the dry air power loss on the TWC wire is given as:

$$P_{TWCdry} = 0.00998(T_{sense} - T_{ambient}) \cdot (\frac{P_{ambient} \cdot TAS}{T_{film}+273.15})^{0.2325} \quad (16)$$

3.3 Analysis of Sensor Responsiveness in Wind Tunnel

Data was collected in test points, where the wind tunnel spray was turned on for a specified period of time (generally two minutes) while the aerodynamic and icing cloud conditions in the wind tunnel were held constant. The test points were completed at a variety of pressures, temperatures, droplet sizes and true air speeds. An algorithm to isolate these test points from the recorded data was implemented as follows.

In order to find test points, the time instances at which the spray was turned on and off were determined. If the spray was turned on for longer than 30 seconds then it was considered a test point. If the spray is turned on for less than 30 seconds, it becomes difficult to gather meaningful data due to the response time of the sensor. A list of test points found using this method was compared with the test matrix, in order to confirm that there were no accidental and undesired points being considered.

In each of these test points, an average LWC, TWC, AIWT WC, MVD, TAS, ambient pressure and ambient temperature were determined by taking a simple mean. The standard deviation of each of these values was also taken and considered as the measurement uncertainty. Adjusting these averages for response time is necessary, as otherwise the WC is underestimated and uncertainty is overestimated. At the beginning of each test point, the sensor WC is underestimated compared to the nominal WC and the sensor WC spikes when the spray is turned off. This appears to be due to a mechanical response of the wind tunnel when the valve closes and thus must be accommodated for. The first 15 seconds and last 10 seconds of each test point were removed from the calculations of the averages and standard deviations in order to accommodate for the sensor response time.

The data were then organized into two types of sweeps using an algorithm. First, there were LWC sweeps where the AIWT WC was varied but the points were selected with an MVD within 10 % of a desired value and the TAS within 5 m/s of a desired value. The other type of sweeps were MVD sweeps where the MVD is varied and points were selected with an LWC within 15 % + 0.02 g m^{-3} of a desired value. In section 4, the results from five sweeps in the ICD tests and six sweeps in the Nevzorov tests are presented. The sweep types and variables are shown in Table 2, and the scatter plots of these sweeps are shown in section 4. An expanded table, showing each test point is given in Appendix D.

Table 2. MVD and LWC sweeps information.

Sensor	Sweep Type	MVD	AIWT WC	TAS
Both	LWC	10μm	0.5g/m^3-2.0g/m	90m/s
Both	LWC	20μm	0.5g/m^3-3.0g/m^3	80m/s
Nevzorov	LWC (Pressure set to 70kPa)	20μm	0.5g/m^3-3.0g/m^3	80m/s
Both	LWC	100μm	0.25g/m^3-1.0g/m^3	80m/s
Both	LWC	250μm	0.5g/m^3-1.0g/m^3	80m/s
Both	MVD	30μm-250μm	0.2g/m^3	100m/s
Both	MVD	30μm-255μm	0.2g/m^3	90m/s
Both	MVD	15μm-250μm	0.5g/m^3	80m/s
Both	MVD	10μm-30μm	0.5g/m^3	90m/s
Both	MVD	10μm-230μm	0.7g/m^3	80m/s
Both	MVD	10μm-235μm	1.5g/m^3	90m/s

4. Results and Discussion

4.1 Sensor Responsiveness in LWC Sweeps

The WC detected by hot-wire probes depends heavily on the size of the droplets at all WC values. One way to demonstrated this through the LWC sweeps, which group the data based on the droplet size. The smallest LWC Sweep performed was with a droplet size of 10μm as shown in figure 2.

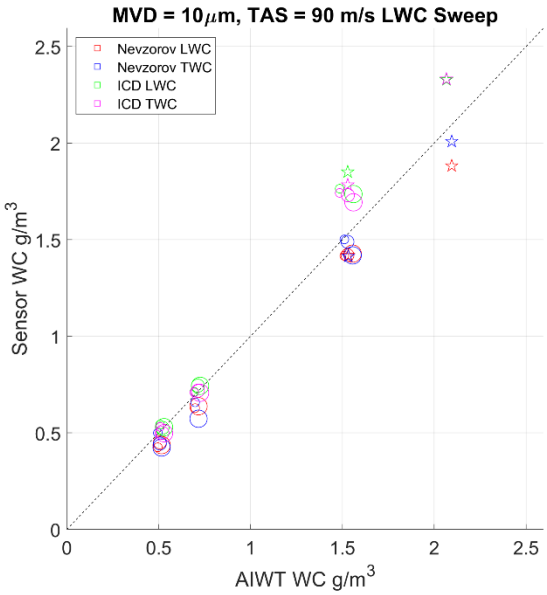

Figure 2. Scatterplot showing the responsiveness of the sensors at various wind tunnel LWC settings with AIWT MVD set to 10 μm. The pressure at these points varies from 40 kPa to 60 kPa, with the pressure being displayed by the size of the marker. The temperature varies from -5°C (shown as stars) to -10°C (shown as circles). The black dashed line is a 1:1 line.

For the Nevzorov, the measured WC relative to the AIWT WC is the smallest at an MVD of 10 μm for the TWC sensor. The collection efficiency of the TWC sensor for MVD of 10 μm was discussed in section 3.2, and is adjusted for in figure 2. When adjusting for the differences in collection efficiency, the measured WC relative to AIWT WC at 10 μm rises from 72 % to 97 % for the TWC sensor. The LWC was not adjusted for a known collection efficiency and is measured as 90% of the AIWT values. This is the highest that the Nevzorov LWC measures relative to the wind tunnel nominal value throughout the LWC Sweeps. The ICD probe does not see the same decrease in detected WC in small droplet conditions as the Nevzorov probe. At an

MVD of 10 µm, the LWC sensor measures 122 % of the AIWT WC and the TWC sensor measures 123 % of the AIWT WC.

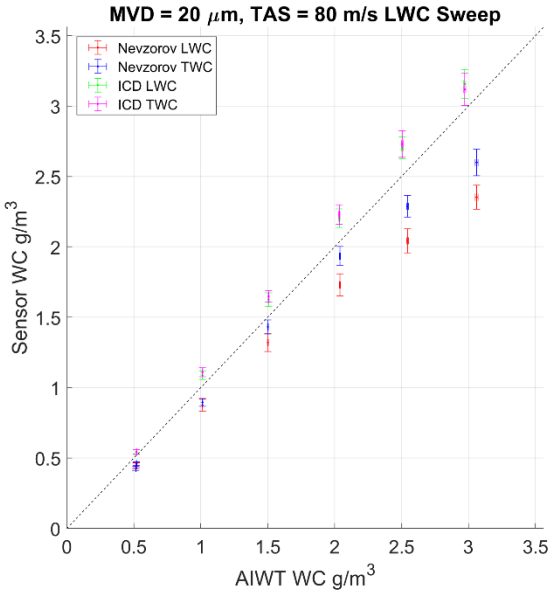

Figure 3. Scatterplot showing the responsiveness of the sensors at various AIWT LWC settings with tunnel MVD set to 20 µm. The pressure at these points is held constant at ground level. The temperature is also held constant at -5 °C. The black dashed line is a 1:1 line. The error bars show the stability of the AIWT WC and sensors.

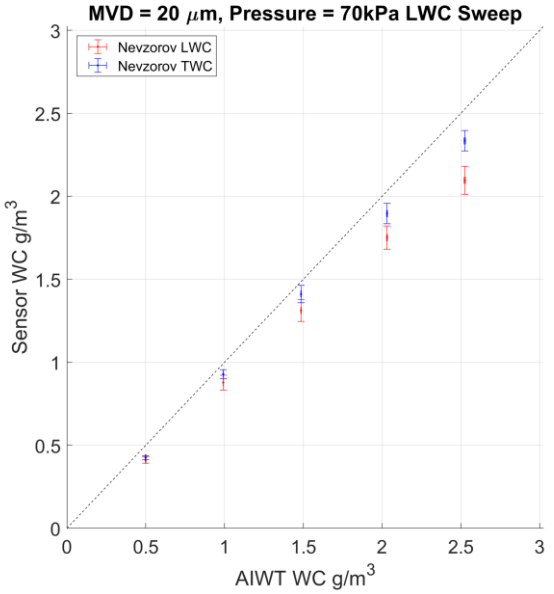

Figure 4. Scatterplot showing the responsiveness of the sensors at various AIWT LWC settings with tunnel MVD set to 20 µm. The pressure at these points is held constant at 70 kPa. The temperature is also held constant at -5 °C. The black dashed line is a 1:1 line. The error bars show the stability of the AIWT WC and sensors. This sweep was only performed for the Nevzorov probe.

At a particle size of 20µm, the two sensors on the Nevzorov both measure slightly lower than the wind tunnel nominal values as shown in figures 3 and 4. The Nevzorov LWC measures 84% of the wind tunnel nominal value, and the Nevzorov TWC measures 89%. For the ICD in figure

3 the results at 20 µm measure closely to one another, with the LWC reading 107 % and the TWC reading 108 % of the AIWT WC.

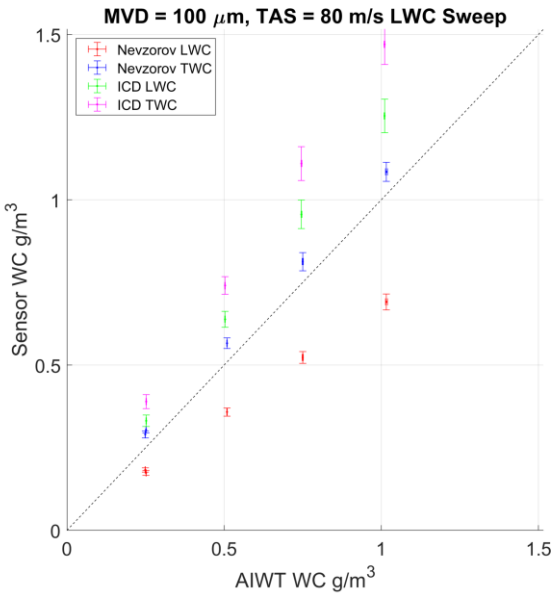

Figure 5. Scatterplot showing the responsiveness of the sensors at various wind tunnel LWC settings with tunnel MVD set to 100 µm. The pressure at these points is held constant at ground level. The temperature is also held constant at -5 °C. The black dashed line is a 1:1 line. The error bars show the stability of the AIWT WC and sensors.

At a droplet size of 100µm in figure 5, there is a more pronounced difference between the LWC and TWC measured by the Nevzorov than with droplets smaller than 100 µm. The TWC measured increases to 112% the AIWT nominal value and the LWC measured decreases to 70% of the AIWT nominal value. This separation between the LWC and TWC is also present in the ICD measurements, with the LWC sensor measuring 123 % and the TWC sensor measuring 143 % of the AIWT WC. The measurements at a droplet size of 100 µm are the highest observed for both ICD sensors in the LWC sweeps.

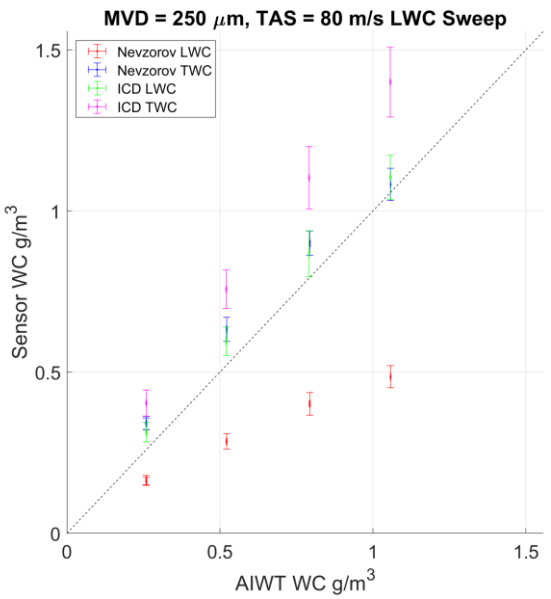

Figure 6. Scatterplot showing the responsiveness of the sensors at various wind tunnel LWC settings with tunnel MVD set to 250 μm. The pressure at these points is held constant at ground level. The temperature is also held constant at -5 °C. The black dashed line is a 1:1 line. The error bars show the stability of the AIWT WC and sensors.

In figure 6, the separation between the measured LWC and TWC is still apparent, especially for the Nevzorov probe. At a particle size of 250μm the Nevzorov TWC is measured the highest throughout the LWC sweeps at 120% of the AIWT nominal value, and the LWC the lowest at 55%. The difference is potentially due to the Nevzorov LWC sensor being prone to splashing effects at high MVDs that results in an underestimation of the WC. The TWC sensor is considered less prone to these splashing effects due to the geometry of the sensor (Korolev, 1998). In practice, especially for real-time in-flight data display, the difference between the two sensors at high MVDs may be problematic, as it may lead to false ice detection in pure liquid conditions.

For the ICD probe at a droplet size of 250 μm the LWC sensor is at the lowest value relative to the AIWT WC at 101 % and the TWC sensor reading has been reduced to 128%. The ICD probe also has a large difference in the WC detected between the LWC and TWC sensors in both figures 5 and 6. This may again lead to ice being falsely detected in pure liquid conditions although not as much as for the Nevzorov. The ICD sensors are more consistent with one another in small droplet conditions as shown in figures 2 and 3.

The ICD and Nevzorov probes have significant differences in the measured WC. While the ICD probe consistently read much higher than the wind tunnel readings for both sensors, the

Nevzorov LWC sensor tends to have lower readings than the wind tunnel reading at all MVDs and the Nevzorov TWC sensor tends to be lower than the wind tunnel with smaller droplets and higher with larger droplets. Both ICD sensors tend to measure higher than both Nevzorov sensors at all MVDs except for 250 μm. At a particle size of 250 μm the Nevzorov TWC and ICD LWC are very similar, with the Nevzorov TWC having slightly higher readings. The ICD TWC measures higher than any other sensor at all droplet sizes.

4.2 Sensor Responsiveness in MVD Sweeps

The MVD Sweeps are presented in figures 7-12.

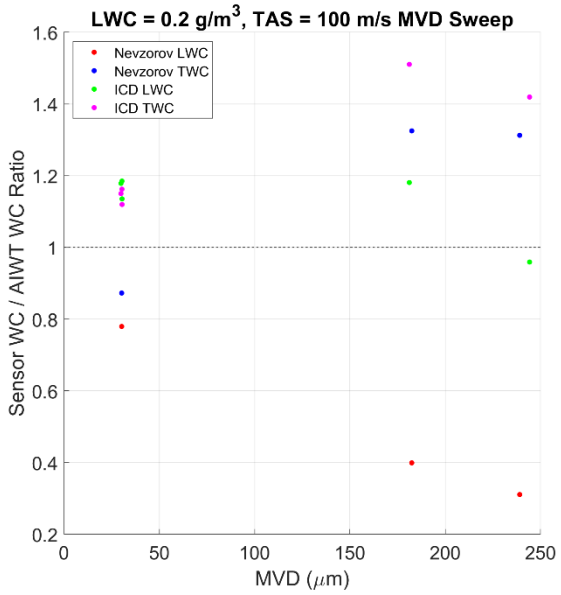

Figure 7. Scatterplot showing the responsiveness of the sensors at an LWC setting of 0.2 g m^{-3} at various droplet sizes settings ranging from 30 μm to 244 μm. The temperature at these points is set to -5 °C, and the pressure is set to ground level pressure. The wind tunnel TAS was set to 100 m/s.

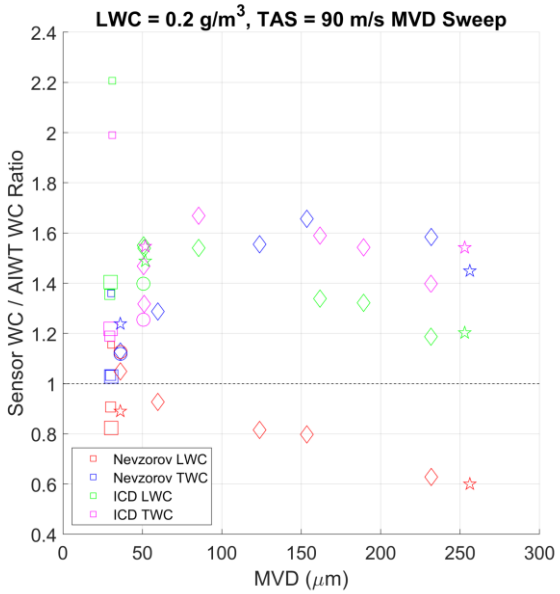

Figure 8. Scatterplot showing the responsiveness of the sensors at an LWC setting of 0.2 g m^{-3} at various droplet sizes settings ranging from 30 µm to 256 µm. The temperature at these points varies from -35 °C to -5 °C, shown as circles at -35 °C, diamonds at -20 °C, squares at -10 °C and stars at -5 °C. The pressure ranges from 40 kPa to 80 kPa which is shown by the size of the markers, with larger markers representing higher pressures. The wind tunnel TAS was set to 90 m/s.

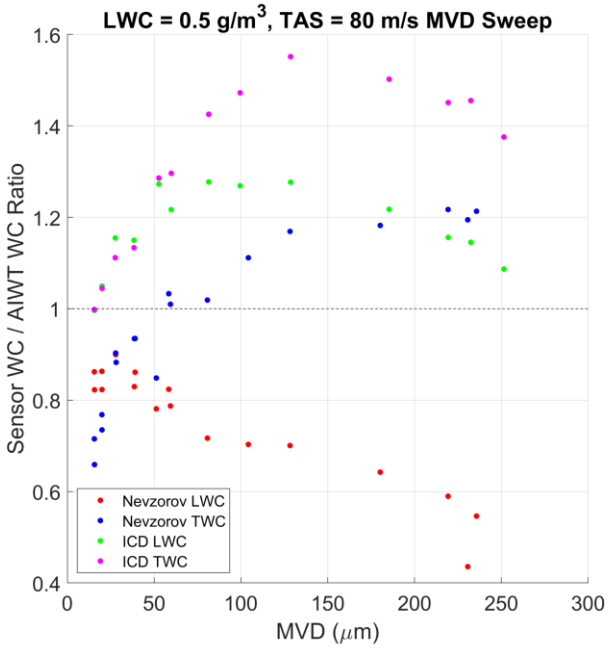

Figure 9. Scatterplot showing the responsiveness of the sensors at an LWC setting of 0.5 g m^{-3} at various droplet sizes settings ranging from 15 µm to 250 µm. The temperature at these points is set to -5 °C, and the pressure is set at ground level. The wind tunnel TAS was set to 80 m/s.

The MVD sweeps have very clear patterns, which vary between sensors. As shown in figures 7 - 9 where the LWC varies from 0.2 g m^{-3} – 0.5 g m^{-3} the Nevzorov LWC / AIWT WC ratio shows a general decreasing pattern as the MVD increases. This pattern is shown in figure 7 with the

LWC / AIWT WC ratio ranging from a maximum 0.78 at an MVD of 30 μm to a minimum of 0.31 at an MVD of 239 μm. Figure 7 has the lowest LWC / AIWT WC ratio observed for the Nevzorov, suggesting that the higher TAS of 100 m/s may lead the splashing effects on this sensor being more pronounced as the other MVD sweeps have TAS ranging from 80 m/s – 90 m/s. The Nevzorov TWC / AIWT WC ratio has a pattern of generally increasing as the MVD increases up to an MVD of around 150 μm. At droplet sizes larger than 150 μm, the TWC / AIWT WC ratio decreases slightly as MVD increases in figures 7 and 8 and increases slightly in figure 9.

A drop-off of the measured LWC / AIWT ratio with droplets with sizes above 130 μm is a consistent pattern for the ICD in figures 7-9, with the pattern being most prominent with the TWC sensor. A similar pattern has also been previously observed in the AIWT in King-Steen et. al. (2021), which presents the performance of a SEA multiwire probe TWC sensor in the AIWT. They observed an increase in the measured LWC/AIWT ratio as droplet sizes increased up to a peak of 1.53 at an MVD of 126 μm. Figure 9 follows a very similar distribution for the ICD TWC sensor, which had a peak value 1.55 times the wind tunnel nominal value at an MVD of 128 μm. The value then dropped to 1.38 times the wind tunnel nominal value at an MVD of 251 μm. The LWC sensor WC to the AIWT WC ratio also drops off from 1.28 at 128 μm to 1.09 at 251 μm. The Nevzorov TWC to AIWT water content ratio was a bit more consistent, rising from 1.17 at 128 μm to 1.21 at 236 μm in figure 9. This pattern was different in figure 8 for the Nevzorov TWC, which shows a peak of 1.65 at a particle size of 153 μm, and drops down to 1.45 at 256 μm. Nevzorov LWC readings relative to the nominal AIWT values consistently decreased with larger particles.

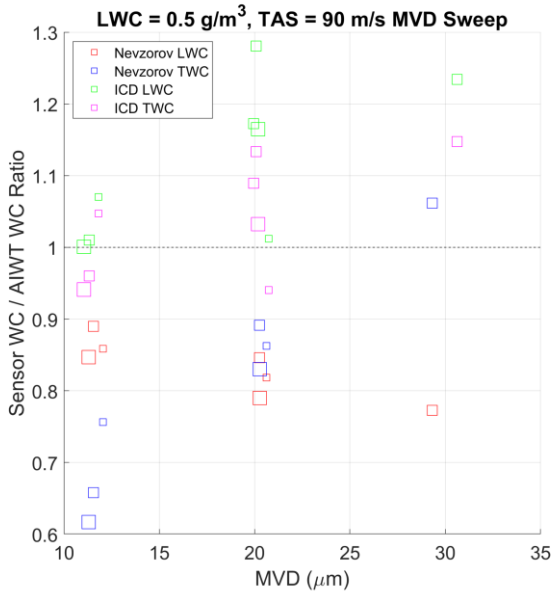

Figure 10. Scatterplot showing the responsiveness of the sensors at an LWC setting of 0.5 g m^{-3} at various droplet sizes settings ranging from 10 µm to 30 µm. The temperature at these points is set to -10 °C, and the pressure ranges from 40 kPa to 80 kPa as shown by the size of the markers, with larger markers representing higher pressures. The wind tunnel TAS was set to 90 m/s.

Figure 10 is unique among the MVD Sweeps, as it covers a very narrow range of particle sizes, from 10 µm to 30 µm. It has the same patterns for each sensor as expected based on figures 7-9. The Nevzorov LWC / AIWT WC ratio decreased as MVD increased in this range, whereas the other 3 sensors all had the sensor WC / AIWT WC ratio increase.

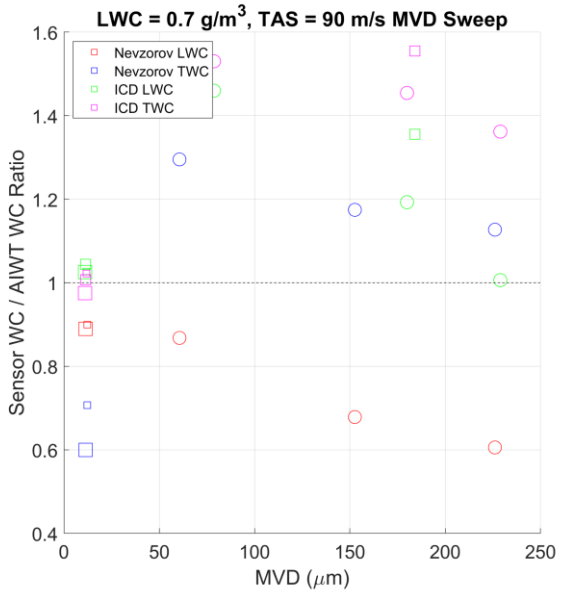

Figure 11. Scatterplot showing the responsiveness of the sensors at an LWC setting of 0.7 g m^{-3} at various droplet sizes settings ranging from 10 µm to 228 µm. The temperature at these points varies from -20 °C to -10 °C, with points at -20 °C being represented by squares and points at -10 °C being represented by circles. The pressure ranges from 60 kPa to 80 kPa as shown by the size of the markers, with larger markers representing higher pressures. The wind tunnel TAS was set to 90 m/s.

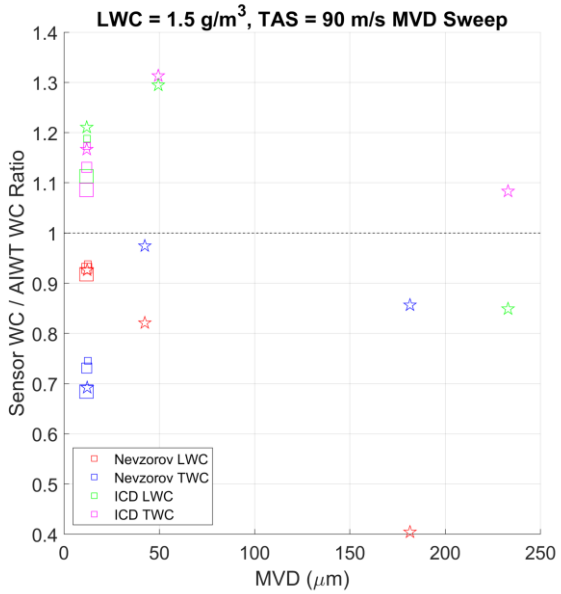

Figure 12. Scatterplot showing the responsiveness of the sensors at an LWC setting of 1.5 g m^{-3} at various droplet sizes settings ranging from 10 µm to 235 µm. The temperature at these points varies from -20 °C to -5 °C, with points at -20 °C being represented by squares and points at -5 °C being represented by stars. The pressure ranges from 60 kPa to 80 kPa. The wind tunnel TAS was set to 90 m/s.

Figures 11 and 12 follow the same general pattern as figures 7 - 9, however there is a clear drop-off in the measured sensor WC / AIWT WC ratio in figure 12 at high MVD (MVD > 150 µm). Here, the Nevzorov TWC / AIWT WC ratio is 0.86 at an MVD of 181 µm, which is lower than in figure 9 where it was 1.18 at 180 µm. Similarly the Nevzorov LWC / AIWT WC ratio is 0.40 at 181 µm, which is lower than figure 9 where it is 0.64. This decrease in sensor WC / AIWT WC ratio compared to figure 9 is prominent in the ICD measurements as well. At an MVD of 232, the ICD had a measured WC / AIWT WC ratio of 1.08 and 0.84 for the TWC sensor and LWC sensors respectively, in figure 9 at 232 µm these ratios are shown to be 1.45 and 1.14 for the TWC and LWC respectively. The difference between the sensor WC / AIWT WC for large-droplets and high WC suggests that splashing effects may be more prominent at these higher water contents.

A recent comparison between these two probes was performed by Lucke et al. (2022), where an 8 mm Nevzorov probe TWC sensor was tested in a wind tunnel where the wind tunnel LWC is based off of ICD measurements. There, the general trend was that the Nevzorov measured lower or equal to the ICD in the 100-150 µm diameter range and higher or equal than the ICD with larger droplets in the 150-300 µm range. If the wind tunnel measurements are based off of the ICD LWC sensor, then this corresponds well with figures 8, 9 11 and 12 which follow the same general patterns.

4.2 Effect of Icing on Nevzorov Probe

One issue that was encountered in the wind tunnel tests is the responsiveness of the reference wires for the TWC and LWC probes to icing. The reference wires serve as a reference to determine the power loss in dry air for the collector wires, so by design they are not supposed to be exposed to hydrometeors. However, ice accretion on the sensor, and other effects, lead to both of these wires experiencing power loss due to ice or water particles. The LWC reference wire appears to have ice accretion, which begins on the side of the probe due to runback water freezing in the glaze ice regime, which grows large enough to touch the wire (see figures 13 and 14). This leads to power loss as the reference wire melts the ice while maintaining constant temperature, and creates an erroneous signal in the data. Another potential cause of power loss on the LWC reference wire is a change in aerodynamics caused by ice accretion on the sensor. The Nevzorov probe is designed to change its angle of attack in order to line up the sensor with air flow, this ensures that the direction of airflow on the sensor is consistent regardless of wind or aircraft pitch. However, ice mass accretion on the sensor leads to a change in the streamlines over the sensor, and thus a change of the angle of attack of the probe. The LWC reference wire may then be exposed to water spray due to the changed angle of attack. From a close inspection of the wind tunnel experiment videos, however, there is no conclusive evidence that the change in the angle of attack is sufficient to explain the false LWC reference signal.

Figure 13. A picture of the Nevzorov probe with icing being seen touching the LWC reference wire during testing.

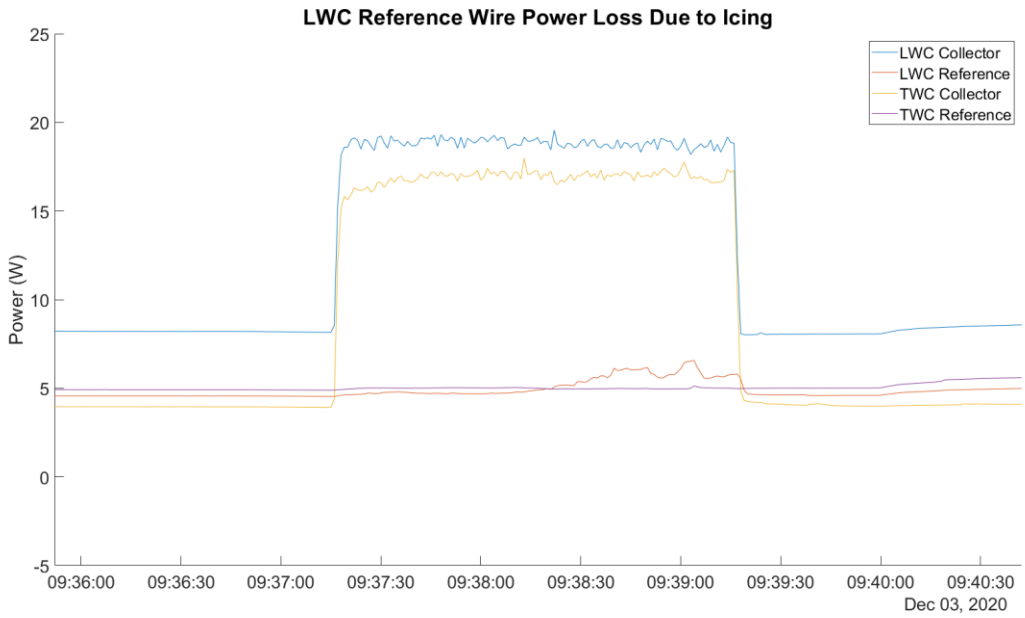

Figure 14. A time-series plot of the power loss on the four Nevzorov wires taken at the same time as the ice is seen in figure 13, with a signal being observed on the LWC reference wire due to the icing. Here, the wind tunnel LWC was set to 1.5 g m^{-3}, the MVD was 10 μm, the TAS was 90m/s, the temperature was -10°C and the pressure was 60 kPa.

Power loss due to spray also occurs on the TWC reference wire but it is less common, and the cause is uncertain. This tends to happen only for small droplets and high LWC at a temperature high enough that the droplets do not immediately freeze. At this point droplets can be observed flowing over the probe, although the video resolution makes it difficult to resolve individual droplets sliding onto the reference cone. It is possible that turbulence around the TWC reference wire causes an eddy which draws small droplets into the reference cone. This effect is more significant at higher LWCs (≥ 1.5 g m^{-3}) and low MVDs (≤ 20 μm). This signal can be seen in Figure 15, which presents the TWC reference wire signal in conditions where the SAT is -5 °C, the LWC is 2 g m^{-3} and the MVD is 10 μm. In this case, the water flowing over the cone does not immediately freeze, and instead it appears that droplets flow from the cylinder onto the TWC reference cone.

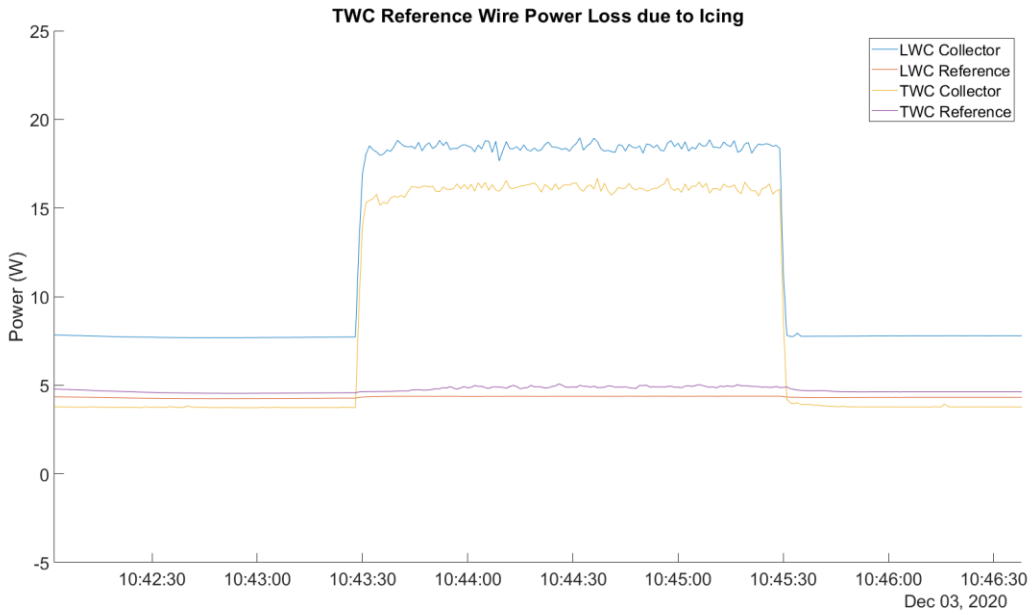

Figure 15. A small signal is shown due to icing on the TWC reference wire in conditions where the temperature is -5 °C, the LWC is 2 g m^{-3} and the MVD is 10 µm.

If droplets flow from the cylinder onto the TWC reference cone, then all points which meet these conditions should show some small effect on the TWC reference wire. One potential phenomenon that can counteract this is ice accreting on the sensor and shielding the reference wire from the air flow and water spray. An example of this supposed interaction can be seen as anti-correlation of false LWC and TWC reference signals in figure 17. From the video taken it is seen that an icicle falls off the sensor surface around 16:09:19, thus stopping the false signal of LWC reference wire and enabling the false signal of the TWC reference cone. This is shown in figures 16a and 16b.

Figure 16. a and b. Photos taken of the sensor before and after a large chunk of ice fell off of the side of the sensor. Depicted is a change in the signal on the reference wires between these two points.

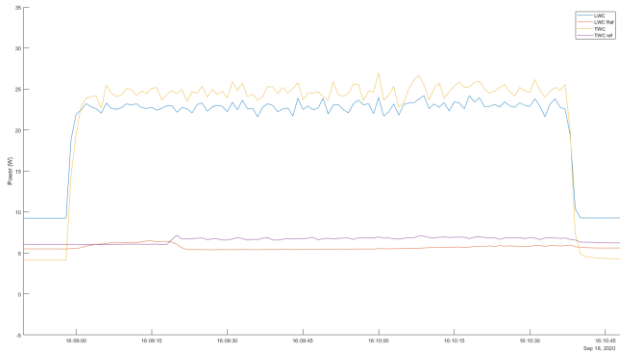

Figure 17. The anticorrelation in the false signals between the LWC and TWC reference wires when the chunk of ice fell off of the sensor at around 16:09:19.

The exposure of the reference wires to water makes them unreliable in realistic icing flight conditions. As the NRC Convair-580 is not equipped with video recorders pointed at the Nevzorov probe, it is unfeasible to manually identify potentially problematic periods with ice accretion on the sensor and filter them out. It is therefore recommended the reference wires be ignored in the calculation of LWC and TWC. Instead, the dry air term should be calculated from ambient parameters (TAS, pressure and temperature) similar to how it is done for ICD and other SEA probes.

4.3 Cloud Masking Unreliability in Nevzorov Calculations

An issue that may be encountered in the processing of flight data is the unsatisfactory algorithm for cloud masking. The traditional way for determining IWC and LWC requires the type of cloud to be known, whether the cloud is liquid, glaciated or mixed phase.

According to the algorithm used, the cloud type is determined to be pure liquid if the two collector wires' power loss agree with one another within 5 %, indicating that they are detecting approximately the same amount of water. In small droplet conditions (MVD < 15 μm), the LWC sensor reads higher than the TWC sensor. In order to ensure the cloud is not misclassified in small droplet conditions with the difference in WC being misattributed to a negative amount of ice, it is necessary to classify the conditions as pure liquid if the LWC collector wire reads higher than the TWC. It is determined to be solely ice if the LWC sensor is detecting 11 % or less of what the TWC sensor detects. This is due to the sensitivity to ice of the LWC collector wire being 11 %. If neither of these two conditions are met, the cloud type is determined to be mixed-phase, containing a combination of both liquid water and ice. If the wires' collection efficiencies

were similar then this would be an accurate way of determining the cloud type, however in this experiment it is apparent that even in all-liquid conditions the two sensors have very different collection efficiencies at different droplet sizes. In large droplet conditions (MVD > 100 μm), the LWC sensor reads low due to splashing effects and so the cloud is classified as mixed phase, with an overestimation of IWC. Even in ideal conditions when the two sensors reasonably agree, for example with 20 μm droplets, noise in the data often leads to the cloud being misclassified as it is common for noise to cause the signals from the two wires to disagree outside the set 5 % threshold at a given point. Overall, this led to 60 % of the in-cloud data being misclassified in the wind tunnel tests, 54 % of the recorded data were misclassified as mixed-phase and 6 % of points as all ice. The remaining 40 % were correctly determined to be liquid phase conditions.

Quantitatively, the misclassification of cloud segments in flight data would lead to an underestimation of LWC of between 10 % (at points considered to have small ice content) to 100 % (at points considered to be pure ice), with the average underestimation being 21 % in comparison to a case where all data is considered as LWC. The TWC is also underestimated due to the difference in the calculation of ice and water. Since some water is misclassified as ice, which dissipates more power to evaporate, the TWC is also underestimated by 6 % on average in comparison to a case where all data is considered as LWC.

As the cloud phase was known in this wind tunnel experiment, the cloud type was hard-coded as liquid (see section 3), so this cloud misidentification did not affect the results. The only time there would be ice in the test section is if an ice build-up on the model or turning vanes shed, which would result in a transient mixed-phase cloud.

4.4 Error Analysis

When considering the experimental uncertainty of the data, both the measurement uncertainty of the sensors and the uncertainty in the AIWT calibrations and control systems must be taken into account. The uncertainty of the AIWT is given in the latest calibration as 6.5 % on the LWC with a LWC stability of 5 % and the MVD measurements have an uncertainty of 10 %, which meets the requirements of SAE ARP 5905.

The sensor uncertainty comes from three primary sources, the stability of the signal, the uncertainty of the dry air fit and the uncertainty present through the calculations. The stability of the signal is observed on the scatter plot error bars, and varies highly with MVD and LWC. Since at higher MVD there is a lower concentration of droplets, there tends to be a higher variance in droplets hitting the sensor, and thus less stability in the LWC. At an MVD of 10 μm, the stability is between 1.7 % - 12.7 % for the ICD LWC sensor, 2.6 % - 11.1 % for the ICD TWC sensor, 1.7 % - 6.4 % for the Nevzorov LWC sensor and 1.4 % - 3.6 % for the Nevzorov TWC sensor. At a higher MVD of 250 μm, the stability for the ICD LWC sensor varies from 6.2 % - 9.6 %, 7.1 % - 10.0 %, for the ICD TWC sensor, 7.1 % - 8.8 % for the Nevzorov LWC sensor and 4.2 % - 5.8 % for the Nevzorov TWC sensor. The next source of uncertainty is the dry air fit that was calculated. The quality of this fit, as discussed in section 3, differs for the four different sensor wires. This uncertainty comes from the mean square error (MSE) on the dry air power loss, which is then propagated to the WC calculations assuming a TAS of 100m/s. The uncertainty from the dry air power loss is summarized in table 3.

Table 3. Uncertainty due to dry air power loss.

Sensor	MSE of Dry Air Power Loss (Watts)	Associated Uncertainty in WC Calculation (g m^{-3})
Nevzorov LWC	0.0097	7.5×10^{-4} g m^{-3}
Nevzorov TWC	0.0067	8.0×10^{-4} g m^{-3}
ICD LWC	0.0064	1.1×10^{-3} g m^{-3}
ICD TWC	0.0061	9.7×10^{-4}

There is also a 5 % uncertainty on the Nevzorov due to the approximation used for the latent heat of evaporation. Overall using the highest observed instability, there is an estimated uncertainty of 10.8 % + 7.5×10^{-4} g m^{-3} for the LWC sensor and 13.8 % + 8.0×10^{-4} g m^{-3} for the TWC sensor on the Nevzorov and an uncertainty of 12.7% + 1.1×10^{-3} g m^{-3} on the ICD LWC sensor and 11.1 % + 9.7×10^{-4} on the ICD TWC (at a TAS of 100 m/s).

These calculated uncertainties account for the difference between the two sensors and differences between the sensor and AIWT measurements with small droplets, shown in figures 2 - 4, but not the higher differences observed with larger droplets shown in figures 5 - 6.

5. Conclusions

The wind tunnel tests give clarity on the performance of the ICD and Nevzorov sensors as a function of both LWC and MVD. It was observed that the Nevzorov TWC tends to have lower readings at low MVD (10-20μm) and higher readings at high MVD (> 100μm). The Nevzorov LWC sensor follows the same general trend, however it reads higher than the TWC sensor at an MVD 10μm, and then falls off as the MVD increases to 250 μm, highlighting the idea that this sensor is likely prone to splashing effects at higher MVDs. The ICD sensors read higher than the Nevzorov sensors at all MVDs, and consistently read above 100 % of the AIWT WCs. They agree with each other very well at low MVD, but the ICD LWC sensor reading tends to fall off more than the TWC sensor at high MVD, leading to a gap between the detected water contents.

These experiments also provide information about how the dry air term should be calculated for the two probes. The formula for the dry air power loss was changed from the formula provided in the user manual, to one that takes into account the temperature of a thin film of air which would appear around the sensor. This refined fit is given in Eq. 7.

This correction improved the fit by approximately 1 % for the ICD LWC sensor, and 7% for the TWC sensor. The dry air term for the Nevzorov is also recommended to be calculated the same way. Even though the variations in conditions can be better measured with the reference wires in ideal conditions, it appears that the reference wires are too unreliable for this purpose of calculating the dry air power loss. In the wind tunnel tests, both reference wires were observed to be prone to losing power due to the presence of water and ice, which is not accommodated in the original design of operation. Unless a way is found to prevent these biases on the reference wires, the data collected from them should be discarded.

Another important observation is that the LWC and TWC sensors measured differently leading to a difference between the calculated LWC and TWC even in liquid phase conditions. With the ICD, the two sensors tend to agree well at low MVD, but diverge at higher MVD where the LWC sensor is more prone to splashing effects. The Nevzorov sensor wires do not agree at low MVDs unless adjusted for the known small-droplet collection efficiency for the TWC sensor. Even when adjusted, splashing effects lead to a large difference between the two sensors at high MVD. This leads to the IWC being overestimated at these higher MVD’s, and potentially negative ice being calculated at lower MVDs where the LWC sensor is more efficient. This

difference should be accounted for in future processing algorithms in order to prevent these issues. As well, long operation of the wind tunnel at sub-zero temperatures may result in ice shedding from the model and turning vanes, circulating briefly through the test section.

Finally, it is recommended that additional tests be conducted with optical array probes to characterize the generated cloud phase (liquid versus mixed phase) and derive LWC quantity from liquid droplet size distributions followed by a comparison with results reported here. It should also be noted that the tests reported here were done in conjunction with the Italian Center for Aerospace Research (CIRA) tests in AIWT, and additional results with the same NRC bulk sensors are reported in Esposito et al. (2022).

Acknowledgments

The authors would like to thank NRC Altitude Icing Wind Tunnel staff: Gislain Chevrette, Shandon Lomoro, Catherine Clark, David Orchard and Peter Forsyth for providing access to and operating the AIWT facility and for review of this report. The authors appreciate support from FRL staff Eric Roux, Daniel MacDonald, and Matthew Bastian on instrument and network set up during the experiments. Help from SEA Inc was critical for software and hardware troubleshooting of M300 DAS and ICD probe. We also thank Walter Strapp for insightful discussions of data processing results and behaviors of the hot-wire probe in diverse conditions. The GLAZEICE project was funded by the APDC program, for which we thank the Program Lead Dany Paraschivoiu.

Appendix A

AIWT flow distribution cross sections for different combinations of TAS, LWC, MVD conditions (LTR-AL-2021-0018).

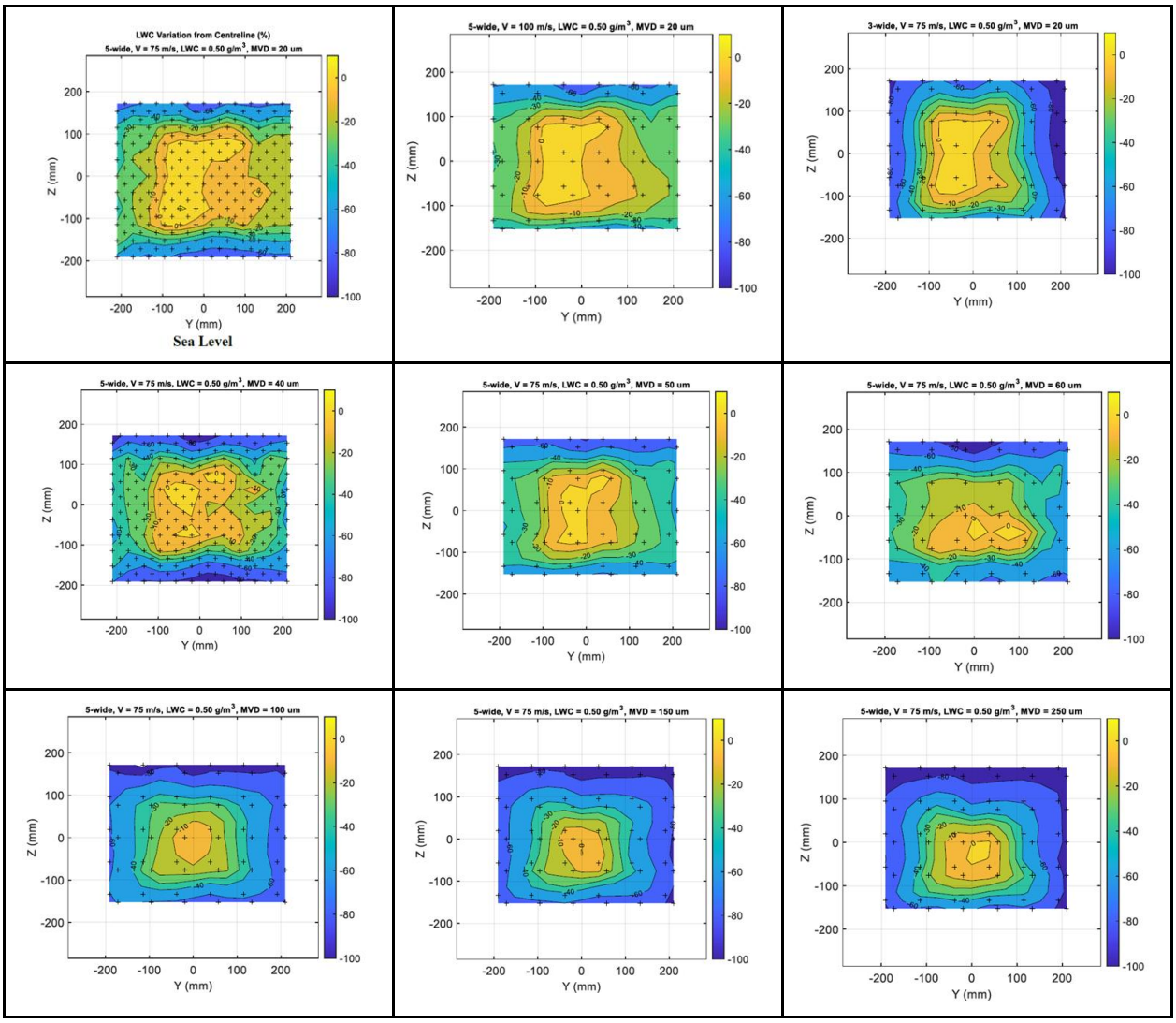

Appendix B

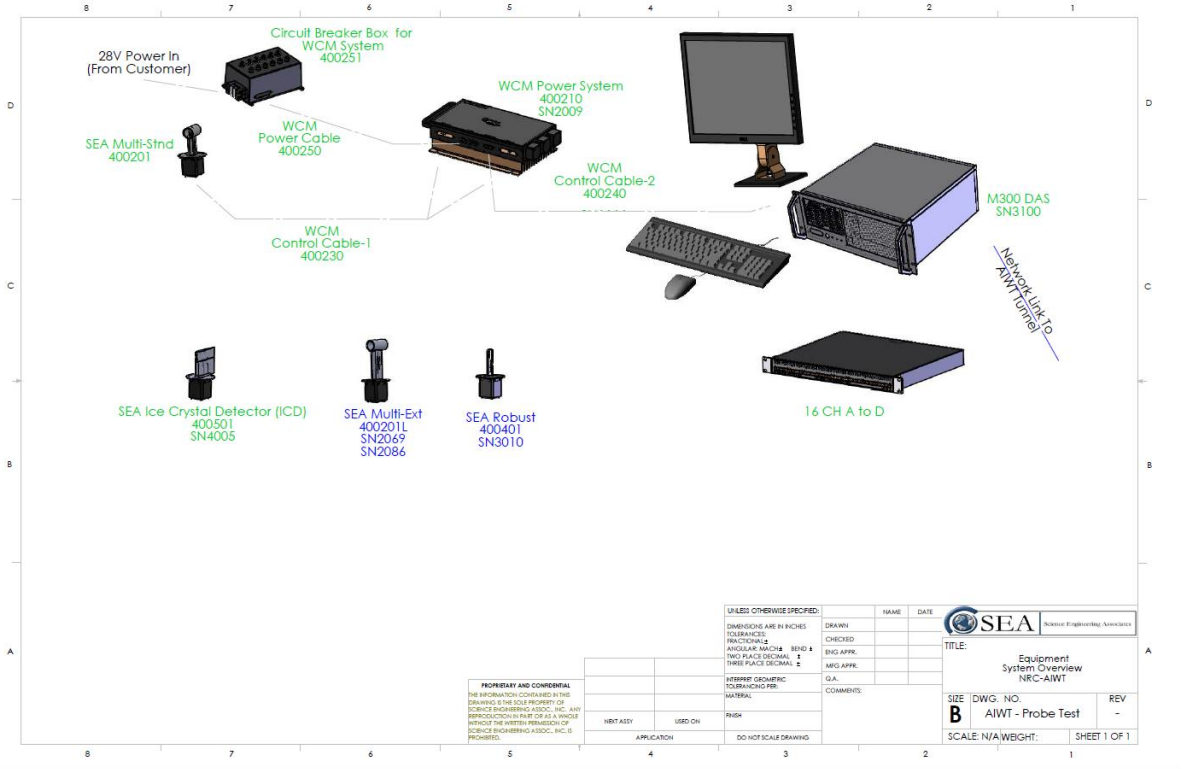

Figure A1. DAS setup.

Appendix C

IVO SENSOR HEAD # SN300

1. Calibration data

	at T (ºC)	R1	R2(coll.)	R3 (ref.)	R4	at T (ºC)
LWC	**23.7**	**1.529**	**2.524**	**1.610**	**1.642**	**23.7**
TWC	**23.8**	**1.582**	**1.532**	**1.701**	**1.520**	**23.8**

	d (mm)	l (mm)	S (cm2)
LWC	**2.0**	**16.2**	**0.324**
TWC	**8.0**		**0.502**

2. User's data

Sensor temperature		**ºC**	**0.0**	**70.0**	**90.0**	**110.0**
LWC sensor	**R_{col}**		2.187	3.182	3.467	3.751
	R_{ref}		1.395	2.030	2.211	2.393
	N_{col}		**1.430**	**2.081**	**2.267**	**2.453**
	N_{ref}		**0.850**	**1.236**	**1.347**	**1.457**
	RS		0.709	1.031	1.123	1.215
TWC sensor	**R_{col}**		1.327	1.931	2.103	2.276
	R_{ref}		1.473	2.143	2.335	2.527
	N_{col}		**0.839**	**1.220**	**1.329**	**1.438**
	N_{ref}		**0.969**	**1.410**	**1.536**	**1.662**
	RS		0.667	0.970	1.057	1.143

Appendix D

Table 4A. Test matrix showing LWC, MVD, TAS, SAT, SP and angle of attack settings of each test point.

LWC, g/m3	MVD, um	TAS, m/s	SAT, deg C	SP, kPa	Angle of attack, deg	Notes
0.42	20	40	-5	100	0	repeat point for ICD (2) and Nz (2)
1.2	28	40	-5	100	0	repeat point for ICD (2)
0.42	20	40	-5	70	0	Nevzorov only
1.2	28	40	-5	70	0	Nevzorov only
0.2	30	80	-5	100	0	Nevzorov only
0.25	250	80	-5	100	0	repeat point for Nz (2)
0.25	100	80	-5	100	0	repeat point for Nz (2)
0.5	314	80	-5	100	0	
0.5	250	80	-5	100	0	
0.5	236	80	-5	100	0	
0.5	187	80	-5	100	0	
0.5	126	80	-5	100	0	
0.5	100	80	-5	100	0	
0.5	80	80	-5	100	0	
0.5	60	80	-5	100	0	
0.5	55	80	-5	100	0	
0.5	40	80	-5	100	0	
0.5	15	80	-5	100	0	repeat point for Nz (2)
0.5	28	80	-5	100	0	
0.5	20	80	-5	100	0	repeat point for Nz (2)
0.75	250	80	-5	100	0	
0.75	100	80	-5	100	0	
1	250	80	-5	100	0	
1	100	80	-5	100	0	
1	20	80	-5	100	0	repeat point for Nz (3)
1.5	20	80	-5	100	0	repeat point for Nz (3)
2	20	80	-5	100	0	

2.5	20	80	-5	100	0	
3	20	80	-5	100	0	
0.5	15	80	-5	70	0	Nevzorov only
0.5	20	80	-5	70	0	Nevzorov only
1	20	80	-5	70	0	Nevzorov only
1.5	20	80	-5	70	0	Nevzorov only
2	20	80	-5	70	0	Nevzorov only
2.5	20	80	-5	70	0	Nevzorov only
3	20	80	-5	70	0	Nevzorov only
0.5	28	80	-5	70	0	Nevzorov only
0.5	40	80	-5	70	0	Nevzorov only
0.5	60	80	-5	70	0	Nevzorov only
0.2	350	90	-5	60	0	
0.2	300	90	-20	60	0	
0.2	200	90	-20	60	0	
0.2	160	90	-20	60	0	
0.2	80	90	-20	60	0	
0.2	50	90	-35	60	0	
0.2	50	90	-20	60	0	repeat point for ICD (2)
0.2	50	90	-5	60	0	
0.2	30	90	-10	60	0	
0.2	30	90	-10	40	0	
0.2	30	90	-10	80	0	
0.5	30	90	-10	60	0	
0.5	20	90	-10	60	0	repeat point for ICD (2)
0.5	20	90	-10	40	0	
0.5	20	90	-10	80	0	
0.5	10	90	-10	60	0	
0.5	10	90	-10	40	0	
0.5	10	90	-10	80	0	
0.7	300	90	-20	60	0	

0.7	200	90	-20	60	0	
0.7	200	90	-10	60	0	ICD only
0.7	200	90	-10	60	30	ICD only
0.7	200	90	-10	60	-30	ICD only
0.7	80	90	-20	60	0	
0.7	10	90	-10	40	0	
0.7	10	90	-10	80	0	
0.7	10	90	-10	60	0	ICD only
0.7	10	90	-10	60	-30	ICD only
0.7	10	90	-10	60	30	ICD only
1.5	350	90	-5	60	0	
1.5	50	90	-5	60	0	
1.5	10	90	-10	60	0	
1.5	10	90	-10	40	0	
1.5	10	90	-10	80	0	
1.5	10	90	-5	60	0	
2	10	90	-5	60	0	
0.2	275	100	-5	100	0	
0.2	200	100	-5	100	0	
0.2	30	100	-5	100	0	repeat point for ICD (3)
0.7	10	100	-5	100	0	
0.2	30	100	-5	70	0	Nevzorov only
0.7	10	100	-5	70	0	Nevzorov only

References

1. Abel S. J., Cotton R. J, Barret P. A., Vance A. K (2014). A comparison of ice water content measurement techniques on the FAAM BAe-146 aircraft Atmospheric Measurement Techniques 7(9): 3007-3022.
2. Bernstein, B., DiVito, S., Riley, J.T., Landolt, S., Haggerty, J., Thompson, G., Adriaansen, D., Serke, D., Kessinger, C., Tessendorf, S., Wolde, M., Korolev, A., Brown, A., Nichman, L., Sims, D., Dumont, C. (2021). The In-Cloud Icing and Large-Drop Experiment Science and Operations Plans [DOT/FAA/TC-21/29]. Atlantic City International Airport, NJ: Federal Aviation Administration, https://doi.org/10.21949/1524472.
3. Clark, C., "LTR-AL-2021-0018 57cm x 57cm Baseline Calibration", March 2021.
4. Cober S.G., and Isaac G.A., (2012): Characterization of Aircraft Icing Environments with Supercooled Large Drops for Application to Commercial Aircraft Certification. Journal of Applied Meteorology and Climatology, 51(2), 265-284.
5. Esposito, M.B., Orchard, D., Lucke, J., Nichman, L., Bliankinshtein, N., Lilie, L.E., and Strapp, J.W.: Comparability of Hot-Wire Estimates of Liquid Water Content in SLD Conditions, SAE Icing Conference, Austria, 2023, submitted.
6. Federal Aviation Administration, 2021: Appendix C to Part 25. U.S. Code of Federal Regulations, Title 14, Chapter I, Subchapter C, Part 25, Appendix C,
7. King-Steen, L. C., Strapp, J. W., Orchard, D., Van Zante, J. F., Korolev, A., Heckman, I., & Esposito, B. (2021). A Preliminary Study of Inter-Facility LWC Differences in Appendix C and Supercooled Large Droplet Conditions due to Calibration Instruments. In *AIAA AVIATION 2021 FORUM* (p. 2652).
8. Korolev, A., Strapp, J. W., Isaac, G. A., & Emery, E. (2013). Improved airborne hot-wire measurements of ice water content in clouds. *Journal of Atmospheric and Oceanic Technology*, *30*(9), 2121-2131.
9. Korolev, A. V., Strapp, J. W., Isaac, G. A., & Nevzorov, A. N. (1998). The Nevzorov airborne hot-wire LWC–TWC probe: Principle of operation and performance characteristics. *Journal of Atmospheric and Oceanic Technology*, *15*(6), 1495-1510.
10. Lilie, L. E., Sivo, C. P., & Bouley, D. B. (2016). Description and results for a simple ice crystal detection system for airborne applications. In *8th AIAA Atmospheric and Space Environments Conference* (p. 4058).
11. Lucke J., Jurkat-Witschas W., Heller R., Hahn V., Hamman M., Breitfuss W., Bora V. R., Moser M. and Voigt C, Icing Wind Tunnel Measurements of Supercooled Large Droplets Using the 12 mm Total Water Content Cone of the Nevzorov Probe (2022).
12. McFarquhar, Greg M., Darrel Baumgardner, Aaron Bansemer, Steven J. Abel, Jonathan Crosier, Jeff French, Phil Rosenberg, et al. "Processing of Ice Cloud in Situ Data Collected by Bulk Water, Scattering, and Imaging Probes: Fundamentals, Uncertainties, and Efforts toward Consistency." Meteorological Monographs 58 (2017): 11.1-11.33.
13. Nguyen, C. M., Wolde, M., Battaglia, A., Nichman, L., Bliankinshtein, N., Haimov, S., Bala, K., and Schuettemeyer, D.: Coincident in situ and triple-frequency radar airborne observations in the Arctic, Atmos. Meas. Tech., 15, 775–795, https://doi.org/10.5194/amt-15-775-2022, 2022.

14. Orchard, D., Clark, C., and Oleskiw, M., "Development of a Supercooled Large Droplet Environment within the NRC Altitude Icing Wind Tunnel," SAE Technical Paper 2015-01-2092, 2015, https://doi.org/10.4271/2015-01-2092.
15. Rigol (2015) M300 Series Data Acquisition/Switch System User Manual
16. Science Engineering and Associates (SEA), (2016) WCM-2000 User Manual
17. Sky PhysTech Incorporated (SPI) Nevzorov hot wire LWC/TWC Probe Operating Manual
18. Strapp, J. W., Oldenburg, J., Ide, R., Lilie, L., Bacic, S., Vukovic, Z. & Leone, G. (2003). Wind tunnel measurements of the response of hot-wire liquid water content instruments to large droplets. *Journal of Atmospheric and Oceanic Technology*, *20*(6), 791-806.
19. King, W. D., Parkin, D. A., & Handsworth, R. J. (1978). A hot-wire liquid water device having fully calculable response characteristics. *Journal of Applied Meteorology and Climatology*, *17*(12), 1809-1813